High-Performance Ultraviolet Photodetectors Based on Controlled Grown ZnO Nanorods and Bu-PPP Heterojunction

Wentao Cheng[a, b, c, d], Xiaopeng Guo[b, c, e], Libin Tang[*b, c], Jinzhong Xiang[*a], Rongbin Ji[b], Ning Wang[f, g] Sin Ki Lai[h], Shu Ping Lau[h]

[a] School of Materials and Energy, Yunnan University, Kunming 650500, China; [b]Kunming Institute of Physics, Kunming 650223, China; [c] Yunnan Key Laboratory of Advanced Photoelectronic Materials & Devices, Kunming 650223, China; [d] Xi'an jingjie Electronic Technology CO. ,Ltd, Xi'an 710075, China; [e] School of Optics and Photonics, Beijing Institute of Technology, Beijing 100081, China; [f] National Engineering Laboratory for Fiber Optic Sensing Technology, Wuhan University of Technology, Wuhan 430070, China; [g] Key Laboratory of Fiber Optic Sensing Technology and Information Processing, Ministry of Education, Wuhan University of Technology, Wuhan 430070, China; [h] Department of Applied Physics, Hong Kong Polytechnic University, Hong Kong SAR, China

ABSTRACT

Currently, the development of UV photodetectors has been hindered by the scarcity of p-type wide band gap materials. Here, a nanostructured ultraviolet photodetector based on the organic/inorganic heterojunction, consisting of the p-type Bu-PPP polymer and n-type ZnO nanorods, is proposed and demonstrated to have high performance. In the heterostructure, both Bu-PPP polymer and ZnO nanorods acted as the light absorber due to their suitable bandgap in the UV region, and the large contact area of the heterojunction facilitated charge transfer. Its current density-voltage behavior was investigated when exposed under different UV light (365 nm) intensities and in the dark. The responsivity of the devices was measured to be as high as 23 A W^{-1} at -1 V bias under UV irradiation. The heterostructure shows huge potential for development of high-performance optoelectronic and optical devices.

Keywords: ZnO nanorods, UV Photodetectors, organic/inorganic heterojunction

1. INTRODUCTION

One-dimensional (1D) nanostructured materials have aroused a vast interest owing to their unique properties and contribution to electronic devices. [1-3] Compared with some typical semiconducting materials such as GaN, SiC and GaAs, zinc oxide (ZnO) stands out due to its large exciton binding energy of 60 meV at room temperature in addition to its solution processability.[4,5] Therefore, ZnO has been widely utilized in many fields, such as piezoelectric nano-generators,[6,7] ultraviolet light emitting diodes (LEDs),[8] sensors,[9,10] solar cells,[11-13] photodetectors [14,15] and so on.

Moreover, 1D ZnO nanostructures (e.g., nanorods) can provide increased surface area for charge transfer and absorption of ultraviolet light when used as electron collectors.[16] Though some ultraviolet detecting devices with inorganic/organic heterojunction based on ZnO nanorods (NRs) are demonstrated with high performance, [17-19] it is still difficult to find stable p-type materials with wide band gap to combine with the n-type ZnO effectively for UV photodetectors (UV PD).

mailto:scitang@163.com; jzhxiang@ynu.edu.cn

Tenth Symposium on Novel Optoelectronic Detection Technology and Applications
edited by Ping Chen, Proc. of SPIE Vol. 13511, 135111G · © 2025 SPIE
0277-786X · doi: 10.1117/12.3055666

Previous reports showed that the polymer, poly (2, 5-dibutoxybenzene-1, 4-diyl) (Bu-PPP), not only can absorb ultraviolet (UV) light, but also has a smooth surface for electron transport.[20, 21] In this work, a novel organic/inorganic UV PD based on Bu-PPP/ZnO nanorods heterostructure were fabricated and characterized, in which both the organic Bu-PPP film and ZnO NRs array were adopted as light absorber. The heterojunction formed between the two components facilitated charge transfer. ZnO NRs array was synthesized by hydrothermal method and was oriented perpendicularly to the substrate, which implies that the carries can effectively transport along the vertical direction. Electrical measurements showed that the UV PD possessed high performance with a responsivity of 23 A W^{-1} and a detectivity of 1.0×10^{12} cm $Hz^{1/2}$ W^{-1}, which revealed great potential for optoelectronic application.

2. RESULTS AND DISCUSSION

2.1 Preparation of ZnO NRs and its structural characterization

All the chemicals were used as-received without further purification. Ethanol (99.8% AR), ethylene glycol (AR) and glacial acetic acid (99.5% AR) were purchased from Chengdu Kelong Chemical Co., Ltd. (Sichuan, China). Ethanolamine (99%-100% AR) was purchased from Tianjin Fengchuan Chemical Reagent Co., Ltd. (Tianjin, China). Zinc acetate dihydrate (99.0% AR) was purchased from Bodi Chemical Co., Ltd. (Tianjin, China). Poly (2, 5-dibutoxybenzene-1, 4-diyl) (Bu-PPP) was purchased from Xi'an Polymer Light Technology Co., Ltd. (Xi'an, China).

Indium tin oxide (ITO) glass substrates (MTI, 30 Ω sq-1) were cleaned in an ultrasonic bath with detergent, acetone and ethanol for 15 minutes each and then rinsed with deionized (DI) water for several times. ZnO sol-gel solution (2 g zinc acetate dihydrate dissolved in a mixed solvent of 60 mL ethanol, 1 mL ethanolamine, 2 mL ethylene glycol and 1 mL glacial acetic acid) was sealed and stored for 12 hrs as the seed solution. Then it was spin-coated (3000 rpm, 60 s) on ITO glass, and heated at 300 ℃ for 2 hrs in the air. For the growth of ZnO NRs on ZnO seed layer, 0.01 M hexamethylenetetramine and 0.02 M zinc acetate dihydrate (molar ratio 1:1) were mixed in DI water for the growth of ZnO NRs. During the hydrothermal growth process, ZnO NRs were grown on the ZnO seed layer in the reaction solution at different temperatures (80, 85, 90 ℃) for 6 hrs, and then naturally cooled to room temperature.

These ZnO NRs substrates were washed for several times with DI water and then dried. Then, the Bu-PPP solution (0.1 g Bu-PPP was dissolved in 1 mL chloroform) was spin-coated on the ZnO NRs array. The Al top electrode was deposited by thermal evaporation. Finally, Au wires were bonded to Al and ITO electrodes using Ag paste to give electrical lead out.

The top-view and cross-sectional view of the ZnO NRs and the ZnO NRs/Bu-PPP heterojuction were characterized by scanning electron microscopy (SEM, Hitachi S-3400N). Ultraviolet-visible-near infrared (UV-Vis-NIR) absorption spectra were measured by a Shimadzu UV-2401 PC spectrophotometer. The Raman spectra were recorded at ambient temperature using a Renishaw inVia Raman microscope with an argon-ion laser of 514.5 nm. The X-ray diffraction (XRD) patterns of the samples were obtained by a Rigaku D/Max-23 diffractometer. The transmission electron microscopy (TEM) and high-resolution transmission electron microscopy (HRTEM) characterizations were performed using the JEOL JEM-2100 TEM. The surface morphology and roughness were studied by atomic force microscope (AFM) (SPA-400). The photoluminescence (PL) emission and photoluminescence excitation (PLE) spectra were recorded by a Hitachi F-4500 spectrometer. The current density-voltage (*J-V*) was tested by a Keithley 2400 source meter under both dark environment and UV light irradiation (λ=365 nm).

Firstly, the growth of the ZnO nanorods (NRs) was investigated. The growth process of ZnO NRs and ZnO NRs/micro-rods are schematically shown in Figure 1a. In order to fabricate different shapes of ZnO NRs, the ZnO seed layer substrates were placed in 0.01 M reaction solution face-down and face-up at 85 ℃ for 6 hrs, respectively. Figure 1b presents the top-view SEM image of the ZnO NRs based on the face-down ZnO seed layer substrates, where uniform ZnO NRs array was obtained. The cross-sectional SEM image of the ZnO NRs is shown in Figure 1c. According to the SEM image, ZnO NRs with the length of ~1.72 μm were synthesized perpendicularly to the substrate. In contrast, both ZnO NRs and micro-rods were co-synthesized on the face-up ZnO growth substrates as shown in Figures 1d and 1e, which suggests that the ZnO NRs were formed from heterogeneous nucleation (preferred orientation) and the micro-rods were formed from homogeneous nucleation (nucleation center). Since the uniform ZnO NRs array with high surface areas and vertical structure is more suitable for homogeneous contact with polymer, it was adopted as the active layer of UV photodetector instead of the ZnO NRs/micro-rods.

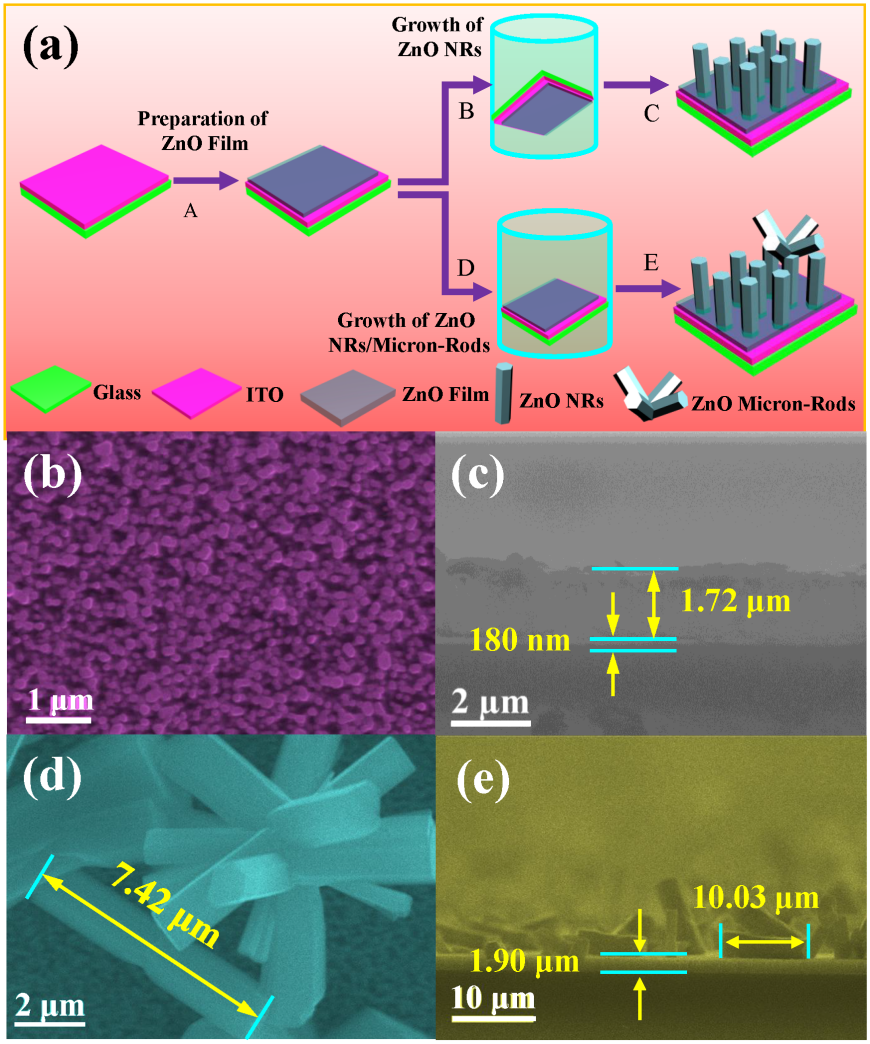

Figure 1 (a) The schematic diagram of the growth process of ZnO NRs and ZnO NRs/micro-rods. (b) Top-view and (c) cross-sectional SEM images of the uniform ZnO NRs array. (d)Top-view and (e) cross-sectional SEM images of the ZnO NRs/micro- rods.

The ZnO seed layer substrates were treated in different conditions for investigating the growth mechanism of the ZnO NRs array. Figure 2 shows the top-view and cross-sectional SEM images of the ZnO NRs array grown on the ZnO seed layer substrate face-down in different concentrations of reaction solution: 0.01 M for Figures 2a and 2c and 0.02 M for Figures 2b and 2d at 80 ℃ for 6 hrs. According to the top-view SEM images in Figures 2a and 2b, the diameters of the ZnO NRs grown in 0.02 M reaction solution ranges from 84-182 nm, which were larger than that growth in 0.01 M reaction solution (55-97 nm). In addition, the increased reaction concentration (i.e. from 0.01 M to 0.02 M) also results in an increased length of ZnO NRs as indicated Figures 2c and 2d.

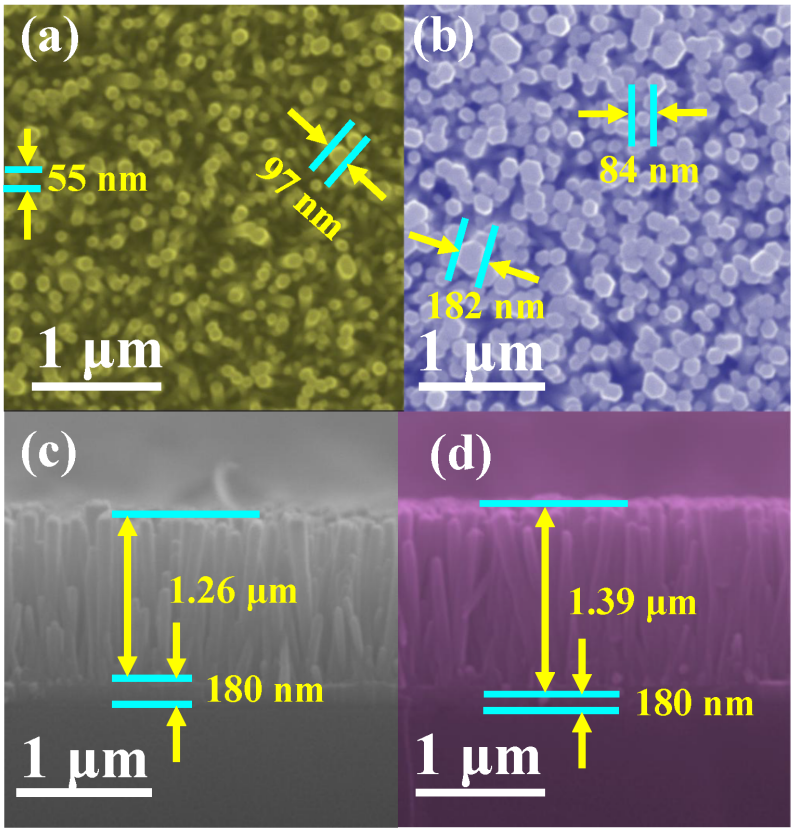

Figure 2 (a) and (b) The top-view SEM images of ZnO NRs grown in reaction solution with different concentrations (0.01, 0.02 M respectively) at 80 ℃ for 6 hrs. (c) and (d) The cross-sectional SEM images of ZnO NRs grown in 0.01 and 0.02 M precursors respectively.

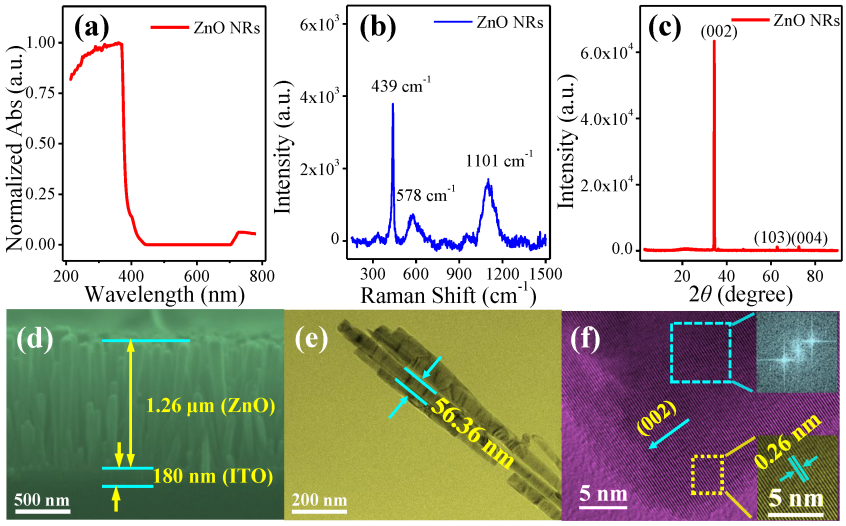

Figure 3 (a) The normalized UV-Vis-NIR absorption spectrum for ZnO NRs. (b) The Raman spectrum and (c) the XRD pattern of ZnO NRs. (d) The cross-sectional SEM image of ZnO NRs array. (e) The TEM image of ZnO NRs. (f) The HRTEM image of a single ZnO NR. Inset: the FFT pattern and magnification of the yellow box.

ZnO NRs played an irreplaceable role in the device since apart from absorbing UV light, it also provided an effective path for the transport of carriers. The UV-Vis-NIR absorption spectrum of ZnO NRs is shown in Figure 3a. The ZnO NRs have a strong absorption in the UV region. The Raman spectra of the ZnO NRs in Figure 3b exhibits three vibrational peaks at 439 cm^{-1}, 578 cm^{-1}, and 1101 cm^{-1}, which corresponds to the E2H, E1L and E1L vibrational modes respectively. [4,22,23] From the XRD pattern of ZnO NRs shown in Figure 3c, it was found that the (002) diffraction peak was much stronger than (103) and (104), indicates that the longitudinal growth of ZnO NRs was preferred, which would enable effective carrier transport along the vertical direction. The wurtzite crystal structure of ZnO was also verified. The ZnO NRs array grown in 0.01 M reaction solution at 80 ℃ for 6 hrs as shown in the cross-sectional SEM image in Figure 3d was scratched from the substrate and observed under TEM as shown in Figure 3e. The diameter of the ZnO NR is about 56 nm. In the HRTEM image of the ZnO NRs shown in Figure 3f, the lattice spacing can be calculated to be 0.26 nm, which corresponds to the (002) peak in the XRD spectrum. [24, 25]

The fabrication process of the UV PD is schematically illustrated in Figure 4a. Figure 4b shows the cross-sectional SEM image of the ZnO NRs/Bu-PPP heterostructure, which indicates that the spin-coated Bu-PPP layer on the top of ZnO NRs was ~550 nm in thickness. Figure 4c is the top view of the ZnO NRs array filled with Bu-PPP. The corresponding AFM image is shown in Figure 4d. The RMS roughness of the Bu-PPP/ZnO NRs is 14.9 nm. Figure 4e is the cross-sectional SEM image of ZnO NRs/Bu-PPP heterostructure with the Al electrode, showing that ~500 nm Al was deposited as the top electrode. Figure 4f is the top view of the Al film deposited on the ZnO NRs/Bu-PPP layer and its corresponding AFM image is shown in Figure 4g. From the two images, it can be observed that the deposited Al electrode presents a smoother surface with the RMS roughness decreases to 1.8 nm.

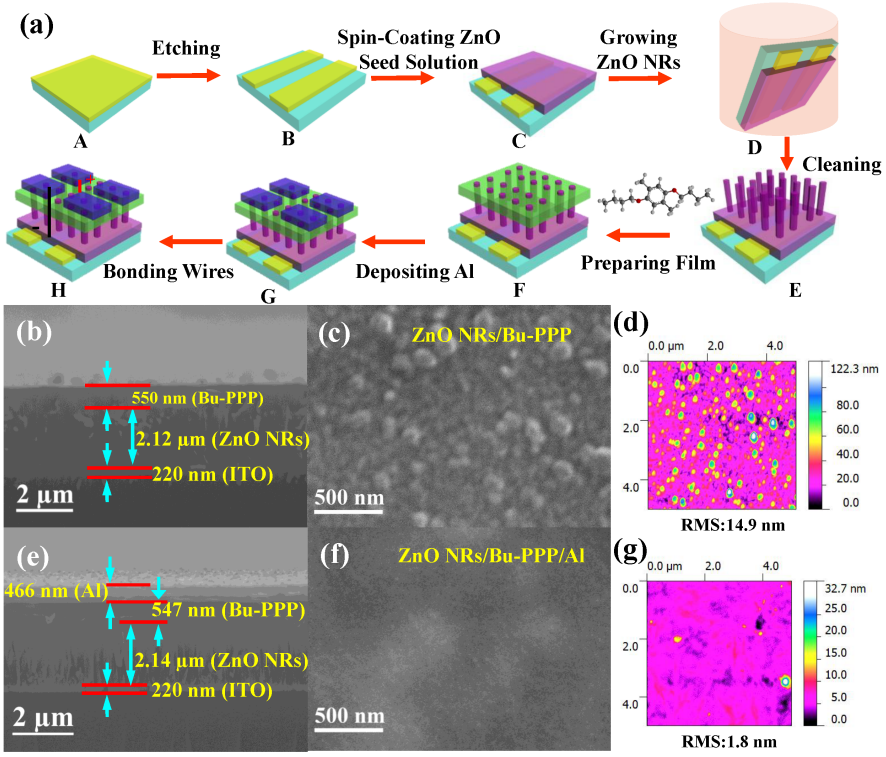

Figure 4 (a) The schematic illustration of fabricating the ZnO NRs/Bu-PPP heterostructure UV PD. (b) The cross-sectional and (c) the top- view SEM images of ITO/ZnO NRs/Bu-PPP functional layer. (e) The cross-sectional and (f) the top-view SEM images of ITO/ ZnO NRs/Bu-PPP/Al. (d) and (g) are the AFM images of the ITO/ZnO NRs/Bu-PPP and ITO/ ZnO NRs/Bu-PPP/Al respectively.

2.2 Photovoltaic detector performance based on ZnO NRs/Bu-PPP heterostructure

The photoluminescence (PL) and photoluminescence excitation (PLE) spectra for ZnO NRs, Bu-PPP and ZnO/Bu-PPP heterostructure were shown in Figure 5. Figure 5a presents the PL spectrum of ZnO NRs with two emission peaks located at 400 nm and 470 nm when excited by light with various wavelengths (λ_{ex}= 280, 300, 320, 340, 360 nm). In Figure 5b, the Bu-PPP film exhibited two PL emission peaks at 380 and 470 nm, which were resulted from the electron transition back to the ground state [26]. The efficient PL from ZnO NRs and Bu-PPP demonstrate that electron-hole pairs were efficiently generated in both components in the heterostructure under UV illumination. The PL spectrum of the ZnO NRs/Bu-PPP heterostructure shown in Figure 5c exhibits a similar shape and PL peak positions with ZnO, which may be a result of charge transfer between ZnO and Bu-PPP heterojunction such that the radiation recombination from Bu-PPP was significantly quenched. Figures 5d, 5e and 5f are the PL excitation spectra of ZnO NRs, Bu-PPP, and ZnO NRs/ Bu-PPP heterostructure, respectively. Clearly, the heterostructure has the similar PLE spectra shape compared with Bu-PPP, indicating that Bu-PPP mainly contributes to the heterostructure for the PLE spectra.

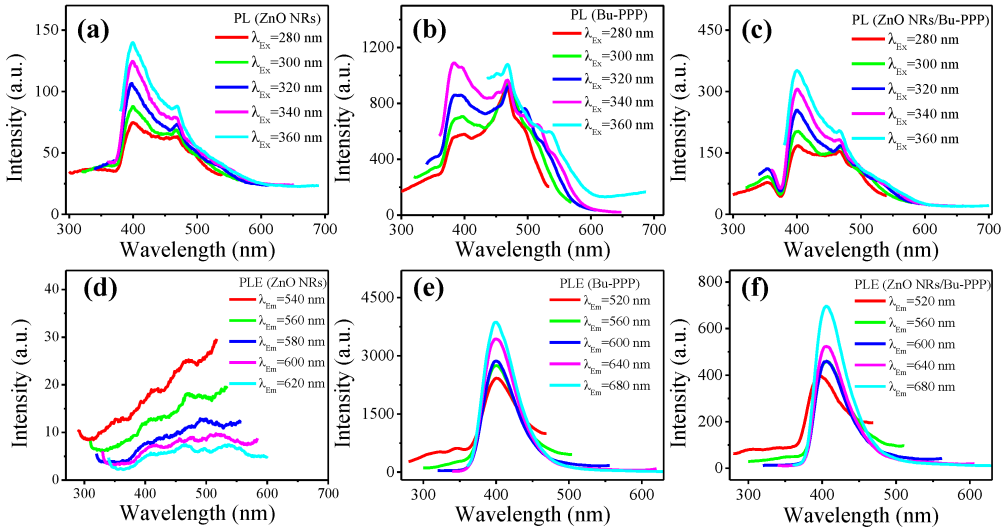

Figure 5 The PL emission spectra of (a) ZnO NRs, (b) Bu-PPP, and (c) ZnO NRs/ Bu-PPP heterostructure. The PL excitation spectra of (d) ZnO NRs, (e) Bu-PPP, and (f) ZnO NRs/ Bu-PPP heterostructure.

To study the properties of the UV PD, the effect of UV illumination intensity (0, 0.06, 0.47, 0.78, 0.95 and 1.45 mW cm^{-2}) on the photoresponse has been investigated. The current density-voltage (*J-V*) are plotted in Figures 6a and 6b, from which it can be obviously found that the photocurrent density increasing with the illumination intensity.

Two important device performance parameters (responsivity and detectivity) of the UV PD have been studied, the responsivity (R) is defined as [27]

$$R=J_{ph}/L_{light}, \quad (1)$$

and the detectivity (D^*) can be calculated as [27,28]

$$D^* =R/(2qJ_d)^{1/2} =(J_{ph}/L_{light})/(2qJ_d)^{1/2} \quad (2)$$

where J_{ph} is the photocurrent density, L_{light} is the incident light intensity, q is the absolute electron charge (1.6×10^{-19} coulombs) and J_d is the dark current density.

R was calculated to be as high as 23 A W^{-1} under 0.06 mW cm^{-2} at -1.0 V bias as shown in Figure 6c. As seen from Figure 6d, D^* reached 1.0×10^{12} cm Hz$^{1/2}$ W^{-1} under 0.06 mW cm^{-2} at -1.0 V bias. The effects of bias voltages and illumination intensities on the device performance were investigated. It was found that R increased with the bias voltage as inferred from Figure 6e. Moreover, D^* has been demonstrated to increase with the bias voltage and decrease with the UV illumination intensities as concluded from Figure 6f.

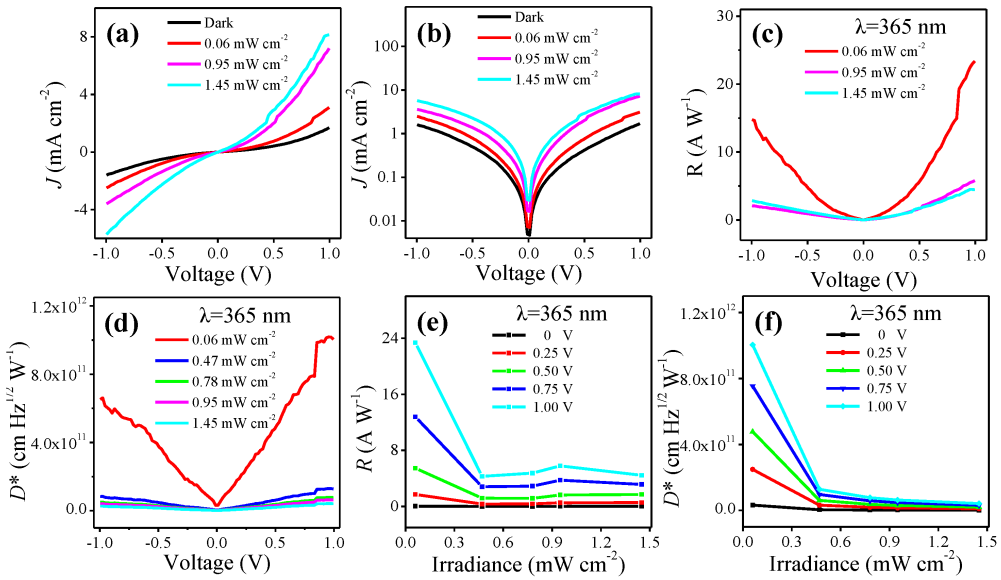

Figure 6 The room temperature device performance of the ZnO/ Bu-PPP UV PD. (a) and (b) are the *J-V* curves of the ZnO NRs/Bu-PPP UV PD in the dark and under a series of UV illumination intensity (λ=365 nm). (c) and (d) The effects of UV illumination intensity (λ=365 nm) on responsivity (c) and detectivity (d). (e) and (f) The effects of bias voltage on the responsivity (e) and detectivity (f).

3. CONCLUSIONS

In summary, high performance UV photodetectors based on the ZnO NRs array/Bu-PPP heterojuction has been fabricated, in which the growth of ZnO NRs had been optimized to enable perpendicular growth onto the ITO substrate, such that an uniform density and diameter of nanorods array can be obtained, which can also provide transfer pathway for charges in the vertical direction simultaneously. Beyond that, polymer Bu-PPP had been introduced for enhancing the absorption of UV light, and also to form a smooth surface for the final deposition of top electrode. The large contacting surface area between the ZnO NRs and Bu-PPP enhanced the charge transfer efficiency. By taking the advantages of the stability of inorganic material and the flexibility of organic material, the UV photodetector has been demonstrated with a big responsivity of 23 A W^{-1} and a high detectivity of 1×10^{12} cm $Hz^{1/2}$ W^{-1}. The various advantages of the heterojuction for UV photodetectors may pave the way for other UV optoelectronics and optics applications.

4. ACKNOWLEDGEMENTS

We acknowledge the financial support from National Key Research and Development Program of China (Grant No. 2019YFB2203404) and Yunnan Province Innovation Team Project (Grant No.2018HC020).

REFERENCES

[1] Xia Y N, Yang P D, Sun Y G et al. “One-dimensional nanostructure: synthesis, characterization and application,” Advanced Materials **34**, 353-389(2003).
[2] Wang Z L “Nanobelts, nanowire, and nanodiskettes of semiconducting oxide-from materials to nanodevices,” Advanced Materials **15**,432-436(2010).
[3] Huang Y, Duan X F, Wei Q Q, et al. “Directed assembly of one-dimensional nanostructures into functional networks,” Science **291**: 630–633(2001).
[4] Özgür Ü, Alivov Y, Liu C et al “A comprehensive review of ZnO materials and devices,” Journal of Applied Physics **98**, 041301.(2005) .

[5] Amari R, Mahroug A, Boukhari A et al "Structural, Optical and Luminescence Properties of ZnO Thin Films Prepared by Sol-Gel Spin-Coating Method: Effect of Precursor Concentration," Chinese Physics Letters **35**, 016801(2018) .
[6] Wang Z L "Towards Self-Powered Nanosystems: From Nanogenerators to Nanopiezotronics" Advance Function Materials **18**, 3553(2008).
[7] Wang Z L, Song J H "Effect of Mn Doping on Solvothermal Synthesis of CdS Nanowires" Science **312**, 242(2006)
[8] Lim J H, Kang C K, Kim K K et al. "UV Electroluminescence Emission from ZnO Light-Emitting Diodes Grown by High-Temperature Radiofrequency Sputtering," Advance Materials **18** 2720(2006)
[9] Wan Q, Li Q H, Chen Y J et al. "Fabrication and ethanol sensing characteristics of ZnO nanowire gas sensors," Applied Physics Letters **84**, 3654(2004)
[10] Mitra P, Chatterjee A P, Maiti H S "ZnO thin film sensor," Materials Letters **35**, 33(1998).
[11] Zhu L P, Wang L F, Xue F et al. "Piezo-phototronic effect enhanced flexible solar cells based on n-ZnO/p-SnS core-shell nanowire array," Advance Science. **4**, 1600185(2017).
[12] Keis K, Magnusson E, Lindström H et al. "Solar Energy Materials and Solar Cells" **73**, 51-58(2002)
[13] Martinson A B F, Elam J W, Hupp J T et al. "ZnO nanotube based dye-sensitized solar cells" Nano Letters **7**, 2183-2187 (2007)
[14] Soci C, Zhang A, Xiang B "ZnO nanowire UV photodetectors with high internal Gain," Nano Letters **7**,1003-1009(2007).
[15] Liang S, Sheng H, Liu Y et al. "ZnO Schottky ultraviolet photodetectors," Journal of Crystal Growth **225**, 110-113(2001).
[16] Rao A D, Karalatti S, Thomas T et al. "Self-assembled, aligned ZnO nanorod buffer layers for high current-density, inverted organic photovoltaics," ACS Applied Materials & Interfaces **6**, 16792-16799(2014).
[17] Sun X W, Huang J Z, Wang J X et al. "A ZnO nanorod inorganic/organic heterostructure light-emitting diode emitting at 342 nm," Nano Letters **8**, 1219-1223(2008).
[18] Lin Y Y, Chen C W, Yen W C "Near-ultraviolet photodetector based on hybrid polymer/zinc oxide nanorods by low-temperature solution processes," Applied Physics Letters,**92**, 233301(2008).
[19] Jiang W, Gao H, Xu L L. "Fabrication and electrical characteristics of individual ZnO submicron-wire field-effect transistor," Chin. Phys. Lett. **29**, 037102 (2012)
[20] Huang J S, Zhang H F, An H Y et al. "Blue electroluminescent diodes utilizing blend of poly(2,5-dibutoxyphenylene) in poly(N-vinylcarbazole)," Chin. Phys. Lett. **13**, 944-946 (1996)
[21] Vahlenkamp T, Wegner G. "Poly(2,5-dialkoxy-p-phenylene)s-synthesis and properties," Macromol. Chem. Phys. **195**, 1933-1952 (1994)
[22] Damen T C, Porto S P S, Tell B "Damen T C, Porto S P S, Tell B. Raman effect in zinc oxide," Physical Review**142**,570-574(1966).
[23] Cheng H M, Hsu H C, Tseng Y K et al 2005 J. Phys. Chem. B 109 8749 "Raman scattering and efficient UV photoluminescence from well-aligned ZnO nanowires epitaxially grown on GaN buffer layer," Journal of Physical Chemistry B **109**, 8749-8754(2005).
[24] Lima R C, Macario L R, Espinosa J W M et al. "Toward an understanding of intermediate- and short-range defects in ZnO single crystals. A combined experimental and theoretical study," Journal of Physical Chemistry A **112**, 8970-8978(2008).
[25] Shen G Z, Bando Y, Liu B D, Golberg D et al. "Characterization and field-emission properties of vertically aligned ZnO nanonails and nanopencils fabricated by a modified thermal-evaporation process," Advanced Functional Materials **16**, 410-416(2005).
[26] Cheng W T, Tang L B, Xiang J Z "An extreme high-performance ultraviolet photovoltaic detector based on ZnO nanorods/phenanthrene heterojunction," RSC Advances **6**, 12076-12080(2016).
[27] Lai S K, Tang L B, Hui Y Y et al. "A deep ultraviolet to near-infrared photoresponse from glucose-derived graphene oxide," Journal of Materials Chemistry C **2**, 6971-6977 (2014)
[28] Guo F W, Yang B, Yuan Y B et a.l "A nanocomposite ultraviolet photodetector based on interfacial trap-controlled charge injection," Nature Nanotechnology **7**, 798-802(2012).